Single dish gradient screening of small molecule localization

Journal:	*Organic & Biomolecular Chemistry*
Manuscript ID	OB-COM-07-2016-001418.R1
Article Type:	Communication
Date Submitted by the Author:	08-Aug-2016

Complete List of Authors:	Beuzer, Paolo; Salk Institute for Biological Studies Axelrod, Joshua; Salk Institute for Biological Studies Trzoss, Lynnie; University of California San Diego Scripps Institution of Oceanography Fenical, William; University of California, San Diego, Professor and Director,Center for Marine biotechnolgy and Biomedicine Marine Research Division, Tumor Growth, Invasion and Metasta Dasari, Ramesh; Texas State University San Marcos, Chemistry and Biochemistry Evidente, Antonio; Universita' di Napoli Federico II, Complesso Universitario Monte Sant'Angelo, Dipartimento di Scienze Chimiche Kornienko, Alexander; Texas State University at San Marcos, Department of Chemistry and Biochemistry Hu, Cang; Salk Institute for Biological Studies La Clair, James; Xenobe Research Institute; University of California San Diego, Chemistry and Biochemistry; Salk Institute for Biological Studies

Organic and Biomolecular Chemistry

COMMUNICATION

Single dish gradient screening of small molecule localization

Paolo Beuzer,[a] Joshua Axelrod,[a] Lynnie Trzoss,[b] Willam Fenical,[b] Ramesh Dasari,[c] Antonio Evidente,[d] Alexander Kornienko,[c] Hu Cang[*,a] and James J. La Clair,[*,a,e,f]

Received 00th January 20xx,
Accepted 00th January 20xx

DOI: 10.1039/x0xx00000x

www.rsc.org/

Understanding trafficking in cells and tissues is one of the most critical steps in exploring the mechanisms and modes of action (MOAs) of a small molecule. Typically, deciphering the role of concentration presents one of the most difficult challenges associated with this task. Herein, we present a practical solution to this problem by developing concentration gradients within single dishes of cells. We demonstrate the method by evaluating fluorescently-labeled probes developed from two classes of natural products that have been identified as potential anti-cancer leads by STORM super-resolution microscopy.

The advent of global approaches offers a suite of methods to rapidly address the biological targets of exogenous small molecules and their regulatory effects at a genetic, epigenetic, proteomic, and metabolomic level, often in unison.[1] It is becoming increasingly evident that a comparative inspection of molecular data with cellular trafficking is vital to understand a molecule's MOA.[2] One can use the direct correlation between cellular selectivity and subcellular localization to further understand the comprehensive responses initiated by a small molecule. In general, the union between cellular and molecular biology is key to fully interpreting the molecule's function.[3]

One of the most challenging problems in addressing small molecule function is understanding the role that concentration plays on the trafficking and subsequent phenotypic responses within a cell.[4] One way to address this problem is to evaluate the phenotypic response to a compound at a single concentration and then develop a screen to identify the effects of concentration. The latter is typically conducted over multiple wells or dishes of cells. Under this approach, one assumes that the tissue or cell culture methods used are identical across the panel of samples. However, this is often not the case. For instance, there are well known but unpredictable experimental biases such as plate side effects as well as adaptations resulting from repetitive cell passages. Furthermore, small molecules often have targets whose expression levels can vary between cultures. If ignored, this issue can lead to experimental evaluation errors, particularly when the target of given molecule is unknown or engages pathways related to cell cycle mediated events, cell-cell interactivity or cell-cell communication.

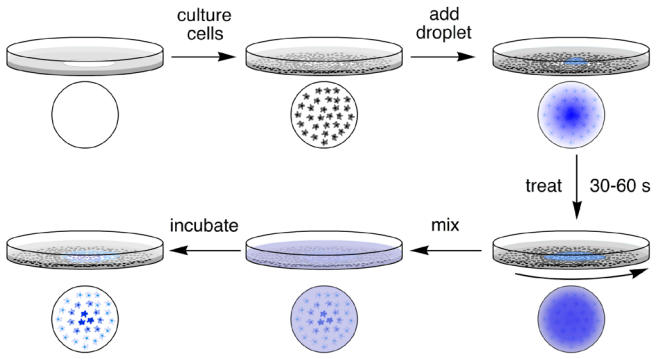

Scheme 1. Schematic representation of the single dish gradient method.

To address this problem, we have developed a practical protocol that evaluates the uptake and trafficking of fluorescent small molecule probes over a concentration gradient within a single dish. As shown in Scheme 1, the process begins by treating a plate of cells cultured to 10^5 to 10^6 cells/cm^2 (Scheme 1). Samples of the probe are generated at 10-50 μM in DMSO. A single drop (3-5 μL) of the DMSO stock is suspended on the tip of a 10 μL pipette and release upon dipping the tip into the media about 1 mm above the cells. The sample is then allowed to sit for 30-60 s at which point the

[a] *The Salk Institute for Biological Sciences, 10010 North Torrey Pines Rd, La Jolla, CA 92037, United States*
[b] *Center for Marine Biotechnology and Biomedicine, Scripps Institution of Oceanography, University of California at San Diego, La Jolla, CA, 92093, United States*
[c] *Department of Chemistry and Biochemistry, Texas State University, San Marcos, TX 78666, United States*
[d] *Dipartimento di Scienze Chimiche, Universita' di Napoli Federico II, Complesso Universitario Monte Sant'Angelo, Via Cintia 4, 80126 Napoli, Italy*
[e] *Department of Chemistry and Biochemistry, University of California at San Diego, La Jolla, CA 92093, United States*
[f] *Xenobe Research Institute, P. O. Box 3052, San Diego, CA 92163, United States*
† Electronic Supplementary Information (ESI) available: experimental procedures. See DOI: 10.1039/x0xx00000x

dish is gently stirred. During this process, the DMSO stock settles to the bottom 'printing' a gradient of compound on the adherent cells on the bottom of the dish.

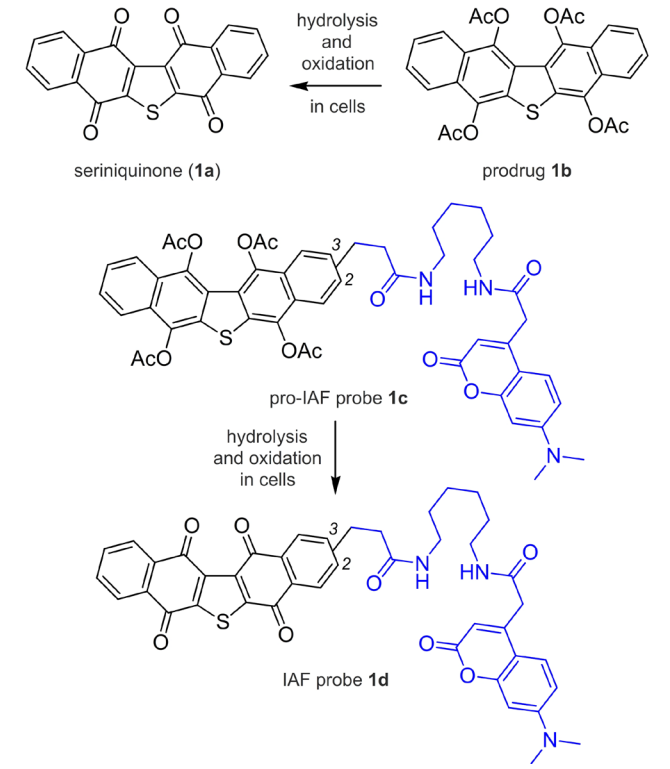

Scheme 2. Structures of seriniquinone (**1a**), prodrug **1b**, pro-IAF probe **1c** and IAF probe **1d**. The synthetic methods used to prepare probe **1c** resulted in an inseparable 6:1 mixture of 2- to 3- substituted analogues, respectively.

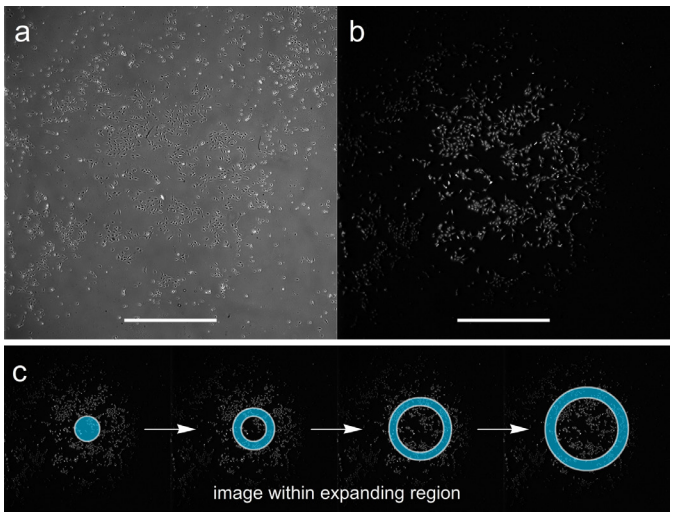

Fig. 1. Exemplary low-resolution image of U2OS (adherent) cells treated with a 5 µL drop of a 50 µM solution of blue fluorescent **1c** in DMSO using the method shown in Scheme 1. The images were collected after incubation for 1 h in DMEM buffer (1 mL) at 37 °C in an atmosphere of 5% CO_2. Both **a)** white light and **b)** fluorescent images were collected at 4x within the same region of cells. **c)** A schematic representation of the imaging method as demonstrated with four concentric disc regions where imaging was conducted. Scale bars denote 1 mm. After treatment and mixing, the media will contain 0.25 µM **1c** and cells containing greater than ~ 1 µM **1c** display fluorescence using this procedure.

To test this concept, we turned to an immunoaffinity fluorescent (IAF) system developed in our laboratories as part of a natural-product drug discovery initative.[5] Our first study explored a recently described pro-IAF probe **1c**, prepared as a fluorescent mimic of prodrug **1b** (Scheme 2).[6] Here, previous studies have shown that the conversion of **1b** to **1a** occurs within tumour cells therein allowing facile delivery **1a**. Comparable, pro-IAF probe **1c** also underwent hydrolysis and oxidation to deliver probe **1d**.[6] As the putative target of these compounds, dermcidin,[6] lacks a detailed function in cells (and hence lacks a viable assay), we were interested in establishing a method to guide the optimization of our prodrug design.

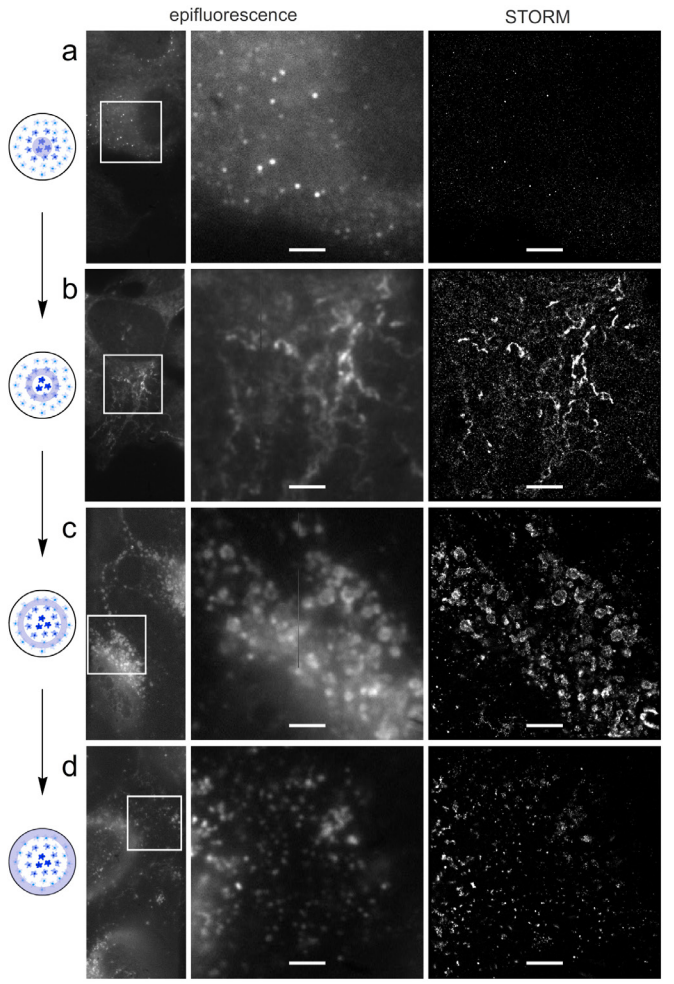

Fig. 2. A different subcellular localization of probe **1c** was observed at increasing radial distances from the centre of treatment (panels **a** to **d**). U2OS cells cultured in an 18 mm plate at 10^6 cells/cm^2 were treated with a 5 µL drop of a 50 µM **1c** using the procedure outlined in Fig. 1. The cells were then incubated in DMEM for 1 h at 37 °C in an atmosphere of 5% CO_2 and fixed. The left column depicts the relative area of the droplet imaged at each row. The central column shows epifluorescence imaging. The right column depicts an expansion of the boxed region using a recently developed STORM imaging technique.[7] The epifluorescence images (excitation filter 590-650 nm, emission filter 663-738 nm) were obtained after immunolabeling for 1 h at 23 °C with 80 µM Alexa647-conjugated anti-IAF TF35 mAb.[8] Scale bars denote 10 µm. Enlarged panels of the STORM images are provided in Supporting Figs. S12-S15.

As shown in Fig. 1, the addition of 5 µL of a 50 µM solution of probe **1c** generated a gradient over a 3 mm diameter region (blue fluorescence, Fig. 1b and Supporting Fig. S11) when

compared the total cell count (white light, Fig. 1a). Using this method, a gradient was generated with the largest dose of **1c** in the centre of the treatment and decreased in dose as one moved towards the edge of the dish. We then imaged the cells within select radii beginning at the centre of the dish and moving outwards (blue shaded regions, Fig. 1c). After examination of multiple plates we found that 4 to 6 regions (four are shown in Fig. 1c) were sufficient to provide a clear and reproducible coverage of each phenotype observed.

Next, we tested the method using a recently developed super-resolution technique for small molecule imaging.[7] In this study, we described the use of a super resolution imaging technique called STochastic Optical Reconstruction Microscopy (STORM). STORM achieves super resolution by identifying the localization of single molecules with sub-nanometric precision. Localization of single molecules can be achieved by labeling the sample with photo-switchable dyes with specific blinking properties that allows for a stochastic activation of a small percentage of fluorescent molecules at a time. When these molecules are separated by a distance that exceeds the Abbe's diffraction limit, their localization can be calculated with sub-nanometer precision by finding the centroid of every blinking event. The final reconstructed image resulting from the sum of the localizations of all blinking events can achieve a final 12-30 nm resolution.

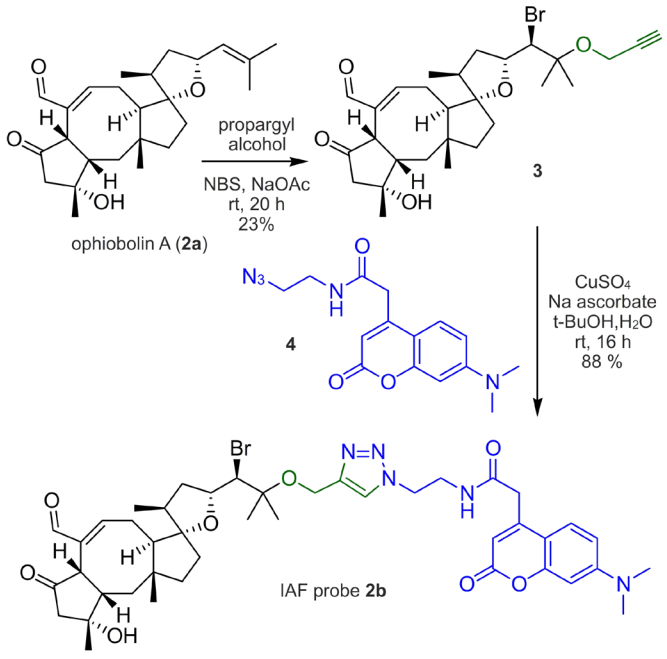

Scheme 3. Synthesis of IAF probe **2b** from ophiobolin A (**2a**).

As illustrated in Fig. 2, we observed strikingly different localization patterns of **1c** corresponding to different radial distances from the centre of the treatment. In the innermost area, corresponding to the highest concentration of **1c**, we observed a pattern characterized by cytoplasmic nanovesicles smaller than 100 nm (Fig. 2a). As we moved farther away from the centre, we could first observe **1c** localizing at thick filaments (Fig. 2b), then at microvesicles (Fig. 2c). Finally, in the outermost part of the droplet, we could detect the compound at smaller and numerous nanovesicles (Fig. 2d).

Based on prior studies,[6] complete conversion of **1c** to **1d** was slower than the 1 h period used for imaging, therefore, the images collected in Fig. 2 arose from a combination of **1c** and **1d**. We are now exploring the use of this method along with parallel LC/MS analysis as a method to guide the development of analogues of **1c** that provide improved pro-drug properties such as optimized rate of delivery, cell selectivity, and pharmacological properties.

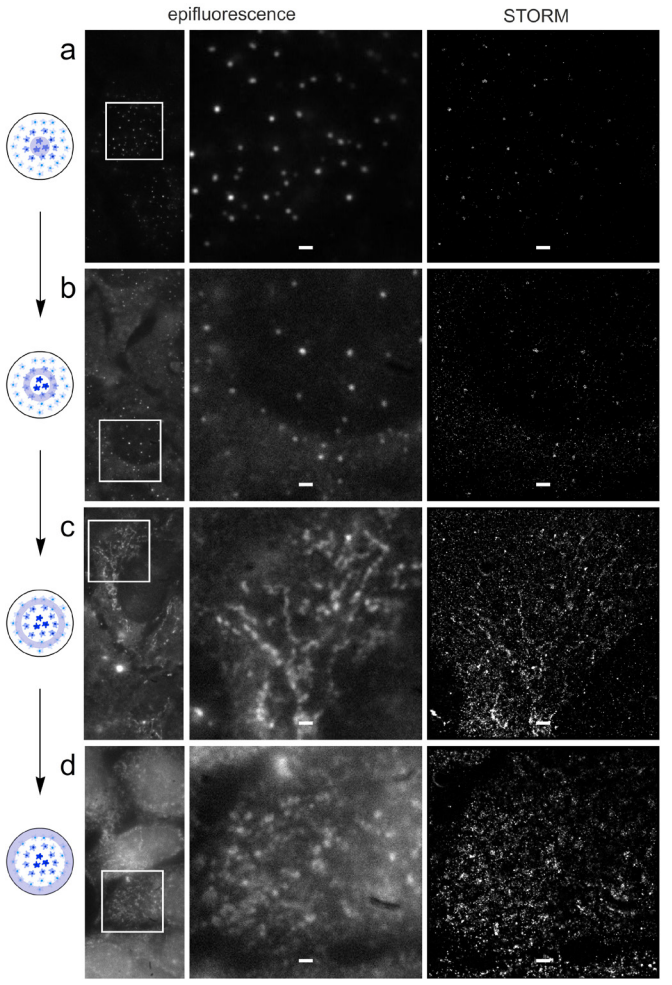

Fig. 3. Different patterns of probe **2b** were observed at increasing radial distances from the centre of the droplet (panels **a** to **d**). U2OS cells cultured in a 18 mm plate at 10^6 cells/cm^2 were treated with a 5 µL drop of 50 uM **2b** using the procedure outlined in Scheme 1. The cells were then incubated in DMEM for 1 h at 37 °C in an atmosphere of 5% CO_2 and fixed. The left column depicts the relative area of the droplet imaged at each row. The central column shows epifluorescence imaging. The right column depicts an expansion of the boxed region using a recently developed STORM imaging technique.[7] The epifluorescence images (excitation filter 590-650 nm, emission filter 663-738 nm) were obtained after immunolabeling for 1 h at 23 °C with 80 µM Alexa647-conjugated anti-IAF TF35 mAb.[8] Scale bars denote 10 µm. Enlarged panels of the STORM images are provided in Supporting Figs. S16-S19.

Our next example focused on an application to a natural product whose MOA we are currently exploring. Ophiobolin A (**2a**),[9] a phytotoxin produced by the plant pathogen *Drechslera gigantea*, offered an excellent model for this study as reports

on its biological activity suggest a diverse array of phenotypic responses. Current reports indicate that **2a** participates in loss of calcium flux,[10] endoplasmic reticulum (ER) stress,[11] induction of apoptosis/paraptosis,[12] as well as inhibition of multiple oncogenic signalling pathways including PI3K/mTOR, Ras/Raf/ERK and CDK/RB.[13] In particular, we were interested in developing methods that would enable us to develop a detailed structure activity relationship (SAR) map that could correlate these phenotypic responses with specific structural features within ophiobolin A (**2a**).[14,15]

We began with the preparation of IAF probe **2b**. Using established methods,[16] we began with the conversion of ophiobolin A (**2a**) into the corresponding α-bromoether **3**, which was obtained as the major stereoisomer (Scheme 3). An IAF tag, azide **4**,[16,17] was then appended to the alkyne terminus of **3** using 1,3-Hüisgen-based Click chemistry, providing probe **2b** in two steps from ophiobolin A (**2a**).[17,18]

Similarly to **1c** (Fig. 2), ophiobolin A probe **2b** (Fig. 3) showed different patterns of localization at different radial distances from the centre of the droplet. In the innermost area, blue fluorescence from **2b** was observed at homogeneously distributed nanovescicles present in both the nucleus and cytoplasm (Fig. 3b). As we observed a slightly more peripheral area of the droplet, we noticed that the majority of these vesicles were localized just outside the nuclear membrane (Fig. 3b). Cells located even further away from the droplet centre, showed that **2b** was localized in thick filamentous structures (Fig. 3c), corresponding to the endoplasmic reticulum (ER). In the outer periphery of the droplet (Fig. 3d), we observed a more diffused cytoplasmic staining where no structure was clearly identified.

In both studies, we observed a clear difference in subcellular localization with respect to probe concentration. In the first study, the subcellular localization of probe **1d** requires metabolic processing of **1c**. The associated lipase and oxidase enzymes that convert **1c** to **1d** are not required to colocalize with dermcidin, the target of the seriniquinone motif in **1d**. Here, probe **1c** and its conversion to **1d** provide an example of an often-neglected facet of small molecule activity and associated bioactivity, namely metabolism.

The localization change of ophiobolin probe **2b** at different concentrations was also not unexpected. The literature already reports dose-dependent phenotypic responses to ophiobolin A (**2a**).[10-14] Furthermore, it is likely that targeting of **2a** and probe **2b** to calmodulin,[19] also plays a complex role in regulating downstream protein binding interactions not only with the ER but also within other regions of the cell. This highlights a second and critical part of small molecule MOA research, namely that few small molecules, natural products in particular, have a single target or single outcome.

Conclusions

While often overlooked, small molecules can reach a multiplicity of targets based on concentration. Understanding a molecule's targets and deciphering the associated phenotypic responses is necessary to develop meaningful assays and evaluate the molecule's activity within this response. The single dish method described in this manuscript offers a practical solution to this problem. While easy to apply, it allows one to conduct detailed studies on the effects of concentration within a single experimental device (glass-bottomed dish). This method provides a more accurate means of controlling experimental parameters, as all cells are cultured using the same nutrients (media) and conditions, It also allows one to rapidly conduct experimentation without the need for large numbers of replications. The latter feature is key to studies that involve time course measurements or complicated imaging techniques. Furthermore, the methods used herein are readily adapted to high-throughput (HT) microscopy,[20] or super-resolution microscopy,[21] as illustrated here by STORM.

Herein, we have demonstrated the method using two examples that contained complex dose-dependent patterns of subcellular localization. Overall, the approach is practical, does not require specialized instrumentation, and can be readily applied to high-content screening and super-resolution methods. Efforts are now underway to use the data obtained in this manuscript to complete the development of the seriniquinone pro-drug motif as well as to elucidate the complex interactivity within ophiobolin A's MOA.

Acknowledgements

This work was generously supported by funding from the Salk Institute (to H. C.), National Institutes of Health (NIH) New Innovator Award 1-DP2-EB020400 (to H. C.), RTEF Career Development Award (to H. C.), Ellison Medical Foundation New Scholar in Aging Award (to H. C.), the Xenobe Research Institute (to J. J. L.), the National Cancer Institute NIH grant CA044848 (to W. F.), the National Cancer Institute NIH grant CA186046 (to A. K.) and the Herman P. and Sophia Taubman Foundation (to W.F.).

Notes and references

1 M. H. Wright, S. A. Sieber, *Nat. Prod. Rep.*, 2016, **33**, 681; M. A. Farha, E. D. Brown, *Nat. Prod. Rep.*, 2016, **33**, 668; C. Wu, H. K. Kim, G. P. van Wezel, Y. H. Choi, *Drug Discov. Today Technol.*, 2015, **13**, 11; M. Kibble, N. Saarinen, J. Tang, K. Wennerberg, S. Mäkelä, T, Aittokallio, *Nat. Prod. Rep.*, 2015, **32**, 1249.

2 Uptake and following subcellular trafficking can often play as large of a role on a small molecules function in a cell as well as its molecular targets. For instance, a molecule that is rapidly translated to the endoplasmic reticulum (ER) via endocytosis would have an effect on proteins within the ER. This could lead to activation of selective targets within the ER with regards to the rest of the cell.

3 J. J. La Clair, *Nat. Prod. Rep.*, 2010, **27**, 969.

4 A. R. Small, R. Parthasarathy, *Annu. Rev. Phys. Chem.*, 2014, **65**, 107; Q. Zheng, M. F. Juette, S. Jockusch, M. R. Wasserman, Z. Zhou, R. B. Altman, S. C. Blanchard, *Chem. Soc. Rev.*, 2014, **43**, 1044; S. van de Linde, S. Aufmkolk, C. Franke, T. Holm, T. Klein, A. Löschberger, S. Proppert, S. Wolter, M. Sauer, *Chem. Biol.*, 2013, **20**, 8; L. M. Wysocki, L. D. Lavis, *Curr. Opin. Chem. Biol.*, 2011, **15**, 752.

5 X. Álvarez-Micó, D. D. Rocha, L. A. Guimarães, A. Ambrose, E. Chapman, L. V. Costa-Lotufo, J. J. La Clair, W. Fenical, *Chembiochem*., 2015, **16**, 2002; L. Farnaes, J. J. La Clair, W. Fenical, *Org. Biomol. Chem.*, 2014, **12**, 418; C. C. Hughes, Y. L. Yang, W. T. Liu, P. C. Dorrestein, J. J. La Clair, W. Fenical, *J. Am. Chem. Soc*., 2009, **131**, 12094; C. C. Hughes, J. B. MacMillan, S. P. Gaudêncio, W. Fenical, J. J. La Clair, *Angew. Chem. Int. Ed. Engl.*, 2009, **48**, 728.

6 L. Trzoss, T. Fukuda, L. V. Costa-Lotufo, P. Jimenez, J. J. La Clair, W. Fenical, *Proc. Natl. Acad. Sci*., 2014, **111**, 14687.

7 P. Beuzer, J. J. La Clair, H. Cang, *Chembiochem*., 2016, **17**, 999.

8 W. L. Yu, G. Guizzunti, T. L. Foley, M. D. Burkart, J. J. La Clair, *J. Nat. Prod.*, 2010, **73**, 1659.

9 T. K. Au, W. S. Chick, P. C. Leung, *Life Sci*., 2000, **67**, 733; P. C. Leung, W. A. Taylor, J. H. Wang, C. L. Tipton, *J. Biol. Chem*., 1984, **259**, 2742; P. C. Leung, L. M. Graves, C. L. Tipton CL. *Int. J. Biochem*., 1988, **20**, 1351; A. Evidente, A. Andolfi, A. Cimmino, M. Vurro, M. Fracchiolla, R. Charudattan. J*. Agric. Food Chem.*, 2006, **64**, 1779.

10 M. Bury, A. Girault, V. Mégalizzi, S. Spiegl-Kreinecker, V. Mathieu, W. Berger, A. Evidente, A. Kornienko, P. Gailly, C. Vandier, R. Kiss, *Cell Death Dis*., 2013, **28**, e561.

11 M. Linxweiler, S. Schorr, N. Schäuble, M. Jung, J. Linxweiler, F. Langer, H. J. Schäfers, A. Cavalié, R. Zimmermann, M. Greiner, *BMC Cancer*, 2013, **13**, 574.

12 M. Bury, E. Novo-Uzal, A. Andolfi, S. Cimini, N. Wauthoz, P. Heffeter, B. Lallemand, F. Avolio, C. Delporte, A. Cimmino, J. Dubois, P. Van Antwerpen, M. C. Zonno, M. Vurro, Y. Poumay, W. Berger, A. Evidente, L. De Gara, R. Kiss, V. Locato V. *Int. J. Oncol*., 2013, **43**, 575.

13 D. R. Bhatia, P. Dhar, V. Mutalik, S. K. Deshmukh, S. A. Verekar, D. C. Desai, R. Kshirsagar, P. Thiagarajan, V. Agarwal, *Nat. Prod. Res*., 2016, **30**, 1455.

14 R. Dasari, M. Masi, R. Lisy, M. Ferdérin, L. R. English, A. Cimmino, V. Mathieu, A. J. Brenner, J. G. Kuhn, S. T. Whitten, A. Evidente, R. Kiss, A. Kornienko, *Bioorg. Med. Chem. Lett*., 2015, **25**, 4544.

15 K. Tsuna, M. Noguchi, M. Nakada, *Chemistry*, 2013, **19**, 5476; D. Xue, Q. Wang, Z. Chen, L. Cai, L. Bao, Q. Qi, L. Liu, X. Wang, H. Jin, J. Wang, H. Wu, H. Liu, Q. Chen, *Bioorg. Med. Chem. Lett*. 2015, **25**, 1464.

16 M. D. Alexander, M. D. Burkart, M. S. Leonard, P. Portonovo, B. Liang, X. Ding, M. M. Joullié, B. M. Gulledge, J. B. Aggen, A. R. Chamberlin, J. Sandler, W. Fenical, J. Cui, S. J. Gharpure, A. Polosukhin, H. R. Zhang, P. A. Evans, A. D. Richardson, M. K. Harper, C. M. Ireland, B. G. Vong, T. P. Brady, E. A. Theodorakis, J. J. La Clair, *Chembiochem*., 2006, **7**, 409-16.

17 W. L. Yu, B. D. Jones, M. Kang, J. C. Hammons, J. J. La Clair JJ, M. D. Burkart, *J. Nat. Prod*., 2013, **76**, 817.

18 K. Horisawa, *Front. Physiol*., 2014, **24**, 457; C. Freidel, S. Kaloyanova, K. Peneva, *Amino Acids*, 2016, **48**, 1357; P. Shieh, C. R. Bertozzi, *Org. Biomol. Chem*., 2014, **12**, 9307.

19 C. K. Johnson, G. S. Harms, *Biochim. Biophys. Acta*. 2016, **1863**, 2017.

20 M. Mattiazzi Usaj, E. B. Styles, A. J. Verster, H. Friesen, C. Boone, B. J. Andrews, *Trends Cell Biol*., 2016, **##,** ### (in press doi: 10.1016/j.tcb.2016.03.008); M. Boutros, F. Heigwer, C. Laufer, *Cell*, 2015, **163**, 1314.

21 J. Molle, M. Raab, S. Holzmeister, D. Schmitt-Monreal, D. Grohmann, Z. He, P. Tinnefeld, *Curr. Opin. Biotechnol*., 2016, **39**, 8; J. B. Grimm, B. P. English, J. Chen, J. P. Slaughter, Z, Zhang, A. Revyakin, R. Patel, J. J. Macklin, D. Normanno, R. H. Singer, T. Lionnet, L. D. Lavis, *Nat. Methods*, 2015, **12**, 244; S. Viswanathan, M. W. Williams, E. B. Bloss, T. J. Stasevich, C. M. Speer, A. Nern, B. D. Pfeiffer, B. M. Hooks, W. P. Li, B. P. English, T, Tian, G. L. Henry, J. J. Macklin, R. Patel, C. R. Gerfen, X. Zhuang, Y. Wang, G. M. Rubin, L. L. Looger, *Nat. Methods*, **2015**, 12, 568; M. K. Lee, P. Rai, J. Williams, R. J. Twieg, W. E. Moerner, *J. Am. Chem. Soc*., 2014, 136, 14003; Q. Zheng, M. F. Juette, S. Jockusch, W. R. Wasserman, Z. Zhou, R. B. Altman, S. C. Blanchard, *Chem. Soc. Rev*., 2014, **3**, 1044; S. van de Linde, S. Aufmkolk, C. Franke, T. Holm, T. Klein, A. Löschberger, S. Proppert, S. Wolter, M. Sauer, *Chem. Biol*., 2013, **20**, 8; H. Jiang, B. P. English, R. B. Hazan, P. Wu; B. Ovryn, *Angew. Chem. Int. Ed. Engl*., 2015, **54**, 1765; J. Chen; J. Gao; J. Wu; M. Zhang; M. Cai; H. Xu; J. Jiang; Z. Tian; H. Wang, *Nanoscale*, 2015, **7**, 3373.